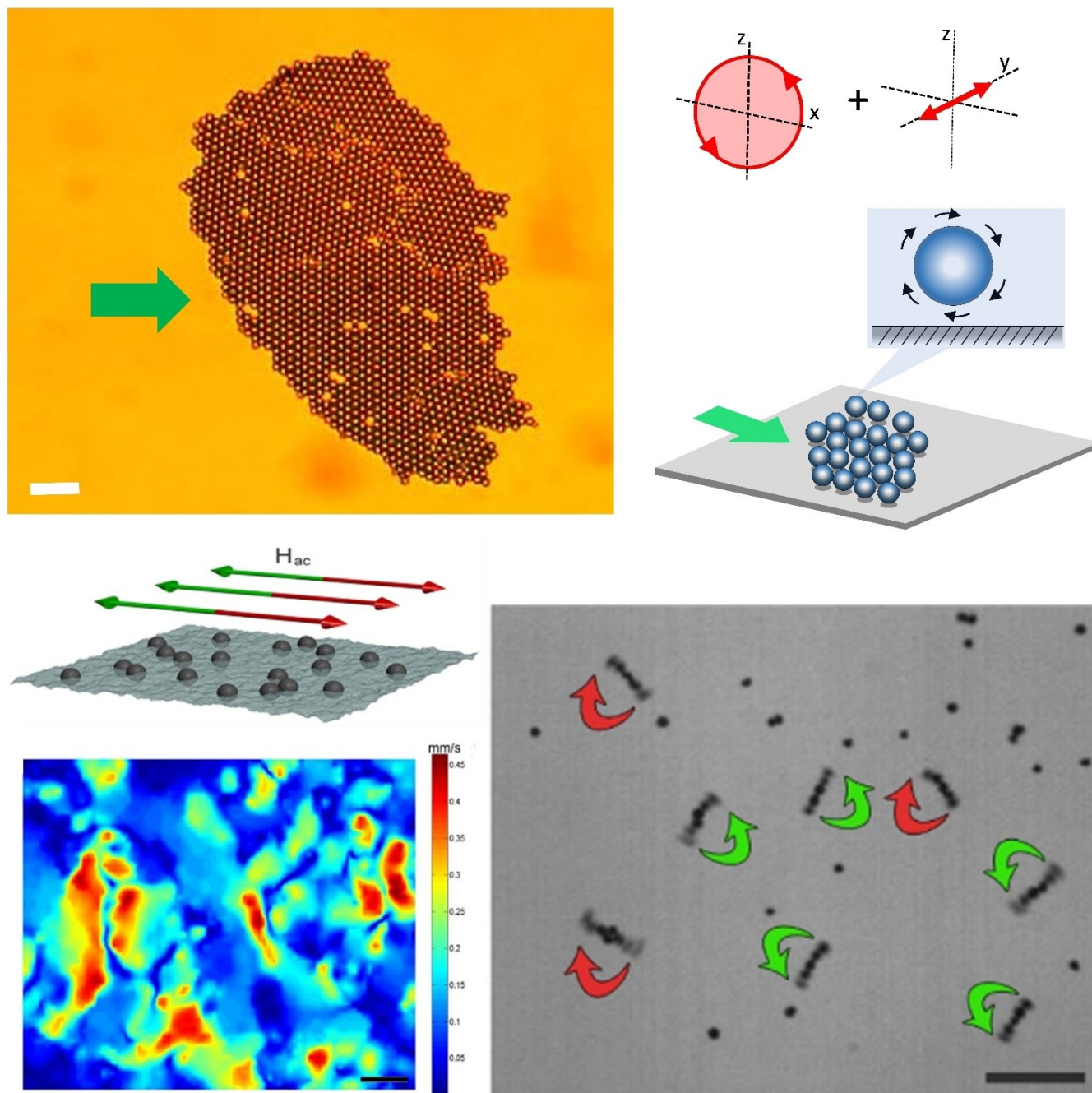Special Collection

Transport and Assembly of Magnetic Surface Rotors**

Pietro Tierno*[a, b, c] and Alexey Snezhko[d]

© 2021 The Authors. ChemNanoMat published by Wiley-VCH GmbH

Abstract: This minireview focuses on recent advances with surface magnetic rotors, namely field-responsive spherical or anisotropic microparticles that translate close to, or are embedded in a confining surface. The application of external magnetic modulations allows these microscopic wheels to be remotely spun and steered while also tuning their interactions and inducing assembly from a collection of disordered, moving units. With optical microscopy one can observe and characterize the complex collective phenomena that emerge in dissipative colloidal systems driven far from equilibrium by external fields. From a technological point of view, magnetic surface rotors envisage implementation into microfluidic devices, and can be used for drug delivery, mixing as well as a model system for biological active matter.

1. Introduction

Soft matter systems, such as colloids, polymers, or liquid crystals, are materials characterized by relatively weak interactions, that can be deformed or controlled via thermal or mechanical stresses.[1] Thus, contrary to other "hard" condensed matter systems, a characteristic feature of soft materials is that they can be manipulated with relatively weak external fields. The same fields may be used to control the interactions between the individual units,[2] to trap microscopic particles against thermal fluctuations,[3] to induce crystallization,[4] melting,[5] or even a net translational motion in a controlled way.[6] In this context, external magnetic fields represent a versatile yet powerful tool to manipulate microscopic colloidal particles,[7] without directly affecting the dispersing medium.

A recent surge of interest in magnetic soft systems has emerged from the prospects of using homogeneous rather than gradient fields to induce particle assembly and transport at the micrometer scale. The development of novel self-propelling microparticles could lead to a deep understanding of the physics of locomotion at such scale.[8] Moreover, magnetic micro rotors may present interesting technological applications as they can be used as efficient microscale mixers, or as steerable drug delivery systems to shuttle biological/chemical cargos directly attached to them or driven by their hydrodynamic flow.

Given their small size, these microdevices operate at a small Reynolds number (*Re*), where inertia is negligible, and the corresponding hydrodynamic laws are time-reversible.[9] Therefore, one must often adopt a special strategy to induce a net translational motion actuating them via homogeneous fields and without using inertia. In some cases, this strategy may be directly inspired by biological systems such as bacteria, that operate at low *Re*. For example, one of the first artificial microswimmers used a red-blood cell attached to a flexible chain of DNA-linked paramagnetic colloids.[10] Such prototype was able to reproduce the bending movement of a flexible flagella, just like bacteria or eukaryotic cells. Since this work, many groups have provided alternative prototypes based on different propulsion schemes.[11]

Here, we overview some recent advances in the field of magnetic surface rotors, rollers and spinners that are microscopic wheels capable of rolling close to a surface or spinning in a viscous fluid. In contrast to other active colloids such as chemically powered ones,[12] the energy supply is provided by an external field[13] which constantly sustains the translational motion. The propulsion mechanism is usually induced by time-dependent fields, weather linearly oscillating,[14] rotating,[15] or precessing[16] ones. More complex three-dimensional modulations have been also used to assemble magnetic matter into complex patterns[17] or to transport particles along predefined paths.[18] Moreover, the applied field often allows such particles to be precisely controlled and steered along a given direction, in contrast to the random excursions displayed by other types of active particles.

Since this is a rapidly expanding research field, it is rather difficult to touch upon all works on the subjects. Thus, we limit this minireview to a few directions and hope that they could provide the reader with a "flavor" of the recent developments in this field. We start this minireview by describing the dynamics of single magnetic rotors in Section 2.1, where we consider isotropic and anisotropic microscopic particles driven by rotating fields and translating at very low *Re*. We discuss the dominant interactions between these particles in Section 2.2, and consider the emerging dynamics that result from the interplay between magnetism and hydrodynamics. In Section 2.3 we introduce ferromagnetic rollers, characterized by non-negligible fluid inertia (thus higher *Re*). Rollers spontaneously select the direction of their propulsion along the surface in contrast to rotors where the direction is prescribed by the driving field. Section 3 is dedicated to the collective assembly of rotors and rollers. In particular, sections 3.1 and 3.2 illustrate the formation of one-dimensional chains and two-dimensional

[a] Dr. P. Tierno
Departament de Física de la Matèria Condensada, Universitat de Barcelona
08028 Barcelona (Spain)
E-mail: ptierno@ub.edu

[b] Dr. P. Tierno
Institut de Nanociència i Nanotecnologia, Universitat de Barcelona
08028 Barcelona (Spain)

[c] Dr. P. Tierno
Universitat de Barcelona Institute of Complex Systems (UBICS)
Universitat de Barcelona, 08028 Barcelona (Spain)

[d] Dr. A. Snezhko
Materials Science Division, Argonne National Laboratory
9700 South Cass Avenue, Argonne, IL 60439 (USA)

sheets of surface rotors, respectively, while section 3.3 describes dynamic states that emerge in ensembles of rollers. In Section 4 we discuss collective phases of magnetic surface spinners. These spinners dynamically assemble from magnetic particles suspended at a liquid interface under oscillating fields. Each spinner rotates around its axis normal to the interface without net propulsion. Finally, in Section 5, we briefly discuss hybrid systems either comprised of active and passive particles or combining different actuation mechanisms. We draw conclusions and discuss perspectives in Section 6.

2. Propelling rotors

2.1. Individual magnetic rotors

The simplest surface microrotor one may think of is composed of a spherical magnetic particle dispersed in a viscous, Newtonian fluid and spinning close to a solid surface. If we consider the same particle in the fluid bulk, its rotational motion alone will not lead to a translation, due to the spatial symmetry of the generated fluid-flow. The solid surface breaks such symmetry and induces a rotation-translation hydrodynamic coupling.[19] We can quantify more this situation by considering a ferromagnetic particle with a permanent moment m, subjected to a torque due to an external rotating magnetic field in the (x, z) plane, with unit vectors (e_x, e_z). Such field can be written as,

$$H(t) = (H_x \cos(\omega t) e_x - H_z \sin(\omega t) e_z) \tag{1}$$

being (H_x, H_z) the field components along the two orthogonal axes, and ω the angular frequency. A circular polarization corresponds to $H_x = H_z = H$, while for an elliptically polarized field one has to further consider the parameter $\beta \equiv (H_x^2 - H_z^2)/(H_x^2 + H_z^2)$ which quantifies the relative importance of one component with respect to the other.

If we assume $\beta = 0$ and negligible thermal fluctuations, the particle dynamics are dictated by the balance between the magnetic torque, $T_m = \mu_m (m \times H)$, and the viscous one $T_v = -\zeta_r \Omega$ that arises from the particle rotation in the fluid. Here μ_m denotes the magnetic susceptibility of the medium, and ζ_r the rotational friction coefficient which account also for the presence of a boundary surface. Solving the torque balance equation, $T_m + T_v = 0$ allows the angular velocity of the particle Ω to be determined. The corresponding drift velocity along the x-axis is given by $v = b f_r(h/b) \Omega e_x$, where b is the particle radius, h stands for the elevation from the surface, and $f_r(h/b)$ is a small correction factor that results from the wall proximity (vanishes for infinite h).

Figure 1(a) shows one example of a field driven microrotor.[20] The latter is made of a ferromagnetic microellipsoid composed of hematite[21] and features a small permanent moment perpendicular to its long axis, $m \sim 10^{-15}$ A m²,[22] see inset in Figure 1(b). The reason why these particles develop a permanent moment perpendicular to their long axis is due to the magnetic structure of hematite.[23]

Pietro Tierno is full professor in the condensed matter physics departement at university of Barcelona. He received his PhD from University of Ulm in 2005. After two post-doctoral stages at Florida State University and at University of Barcelona (UB) he become "Ramon y Cajal" researcher at UB in 2011, and permanent in 2017. His research interests focus on soft condensed matter systems with emphasis on magnetic colloids, propulsion in viscous fluids and geometric frustration phenomena.

Alexey Snezhko received his PhD in Physics and Materials Research from Charles University, Prague, Czech Republic in 2001. After a postdoctoral stay at University of South Carolina he joined the Materials Science Division of Argonne National Laboratory first as a postdoctoral researcher and then as a recipient of the Fermi Fellowship. Since 2008 he has been appointed as a Scientist at Argonne National Laboratory. His recent research focuses on collective dynamics and self-organisation in out-of-equilibrium colloids with complex interactions.
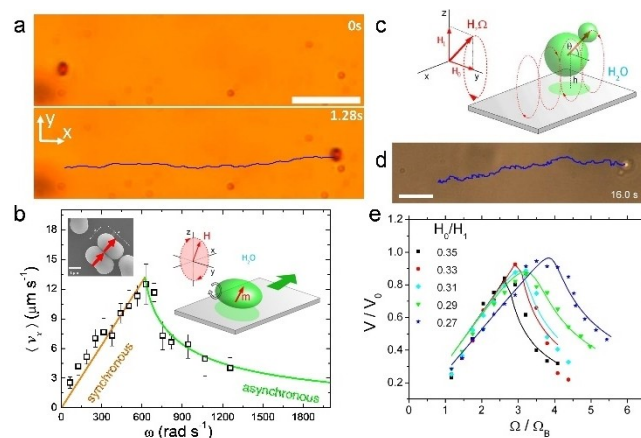
Figure 1. (a) Experimental images showing a ferromagnetic micro ellipsoid driven by a rotating field, scale bar is 5 μm. Reproduced with permission from Ref. [20] (Copyright 2017, Wiley). (b) Average translational speed $\langle v_x \rangle$ versus angular frequency ω for the microellipsoid. Left inset shows a scanning electron microscope image of a pair of particles with depicted the permanent magnetic moments. Right inset shows a schematic of the particle and the rotating field. (c) Schematic of a DNA-linked paramagnetic doublet driven by a magnetic field that performs a conical precession around the y-axis. (d) Microscope image with superimposed the trajectory of a doublet that propels at a speed of $v_x = 3$ μm s⁻¹. Reproduced with permissions from Ref. [27] (Copyright 2010, American Physical Society). (e) Normalized doublet velocity as a function of the rescaled frequency for different values of the relative amplitude H_0/H_1 see Eq. (2). (c–e) Adapted with permissions from Ref. [16] (Copyright 2008, American Physical Society).

Since hematite crystallizes in the corundum form, the Fe cations are aligned antiferromagnetically along this axis. However, above a temperature T~263 K (Morin Temperature), the hematite becomes weakly ferromagnetic, with the magnetic spins lying mostly in the basal plane, i.e. perpendicular to the long axis. Under a rotating field with amplitude $H_0 = 4400$ A·m^{-1} and angular frequency $\omega = 502.6$ rad·s^{-1} this microroller reaches a translational speed of $v_x = 15.6$ μm s^{-1}. Since the field is rotating in the (x, z) plane (Eq. 1), the ellipsoid tends to align its permanent moment along such plane, and thus it rolls perpendicular to its long axis, just like a rolling American football ball.

As shown in Figure 1(b), by increasing the frequency, the average speed displays two regimes of motion. These regimes can be understood by solving the torque balance equation, that predicts how the phase-lag angle ϕ between the permanent moment and the rotating field changes over time. Below a threshold frequency ω_c, the particle moment follows synchronously the rotating field, and ϕ is constant. Thus, $\Omega = \omega$ and the micro-ellipsoid propels at a constant speed, $\langle v_x \rangle = b f_r(h/b)\omega$. For $\omega > \omega_c$, the spinning ellipsoid is unable to follow the fast field rotations, and the phase lag angle continuously increases. In this situation the ellipsoid displays a characteristic "back-and-forth" motion during each field cycle, and its average angular velocity decreases as $\langle \Omega \rangle = \omega - \sqrt{\omega^2 - \omega_c^2}$. Thus, in this "asynchronous regime" its translational speed decreases as well.[24]

Rotating fields can be similarly used to apply a torque to other anisotropic particles, such as magnetic nanorods,[15] paramagnetic microellipsoids,[25] or chain of particles coupled by dipolar interactions.[26] In some cases, a more complex magnetic actuation scheme is required to provide a relative faster propulsion speed. For instance, composite paramagnetic particles with anisotropic shape can reach higher speeds when actuated by an external precessing field than those achieved in a rotating field around the y−axis.[16,27] In the case of Figure 1(c), a doublet made of a small paramagnetic particle (1 micron diameter) linked via DNA to a larger one (2.8 micron) reaches a speed up to 3.5 μm s^{-1} in contrast to 0.6 μm s^{-1} obtained under a simple rotating field. The precessing magnetic field can be written as:

$$\boldsymbol{H}(t) = H_1 \cos(\omega t)\boldsymbol{e}_x + H_0 \boldsymbol{e}_y - H_1 \sin(\omega t)\boldsymbol{e}_z \qquad (2)$$

where H_0 is a static component along the y−axis. Such magnetic modulation induces a gyroscope-like precessional motion of the doublet. The corresponding translational dynamics are characterized by the small particle that performs a circular motion around the centre of mass of the pair, Figures 1(c,d). By measuring the translation speed of this surface rotor one can find again two regimes of motion, see Figure 1(e). At low frequency, the doublet synchronously follows the actuating field, and the velocity raises linearly with ω (in the image the angular frequency is indicated as Ω). At large ω, the doublet still has a constant phase lag with the field, but the high viscous torque forces the small particle to describe smaller orbits. Thus, in contrast to the case of the hematite

propellers, the doublet is still in the synchronous regime and the decrease in speed follows from the reduced rectification induced by the rotating small particle.

2.2. Pair interactions between rotors: magnetism versus hydrodynamics

When considering two surface rotors, the behaviour of the pair results from the balance of difference forces apart from thermal fluctuations and the confining gravitational field. If the particles are not highly charged, as the case of the hematite ellipsoids, one can neglect electrostatic DLVO-like interactions. Thus, the emergent dynamics arise mainly from the interplay between magnetic dipole-dipole forces and hydrodynamics. The first type of interactions can be easily controlled and tuned by the applied field, and thus could be used to measure and test the latter ones. If we consider two point dipoles $(\boldsymbol{m}_i, \boldsymbol{m}_j)$, located at distance $\boldsymbol{r}$, theses interactions are given by:

$$U_{dd}(r) = \frac{\mu_m}{4\pi}\left(\frac{\boldsymbol{m}_i \cdot \boldsymbol{m}_j}{r^3} - \frac{3(\boldsymbol{m}_i \cdot \boldsymbol{r})(\boldsymbol{m}_j \cdot \boldsymbol{r})}{r^5}\right) \qquad (3)$$

and are attractive or repulsive when the moments are parallel or normal to $\boldsymbol{r}$, respectively. For two equal dipoles confined on a plane and oriented by a perpendicular field, $\boldsymbol{H} = H_z \boldsymbol{e}_z$, Eq. (3) reduces to the simple form $U_{dd} \sim m^2/r^3$, and the potential becomes isotropic and repulsive.

More complex is the case of hydrodynamic interactions, namely long-range interactions mediated by the solvent that are excited by the motion of the propellers. These interactions depend on the relative position and orientation of the particles, since the flow field generated by their motion couples them via forces and torques. Thus, it is not possible to describe such interactions via a simple potential term, but one must consider a mobility matrix that connects forces and torques with the hydrodynamic friction coefficients.

Coming back to the experiments, Martinez-Pedrero *et al.* have investigated the interactions between pair of propelling hematite ellipsoids.[28] As shown in Figure 2(a), two different cases are observed when the particles approach each other depending on the driving frequency. For $\omega 300$ rad s^{-1}, the relative arrangement of the particles is dictated mainly by dipolar forces, and the ellipsoids align side by side to line up their permanent moments and to minimize the magnetic energy, first column of Figure 2(b). In contrast, at higher ω, the particles are observed to acquire the opposite configuration, i.e., side by side, column of Figure 2(b). This is also confirmed by measuring the relative orientation angle ϑ, that connects the centre of the two particles and the x−direction. While this configuration is magnetically unfavourable, the strong hydrodynamic flow generated by these rollers give rise to a different dynamic state, that is favoured by hydrodynamic interactions.[28]

One can provide a simple argument to calculate the balance between the two competing forces and the frequency dependence of such states. The attractive dipolar force between two permanent moments m follows from Eq. (3) and it is given by,
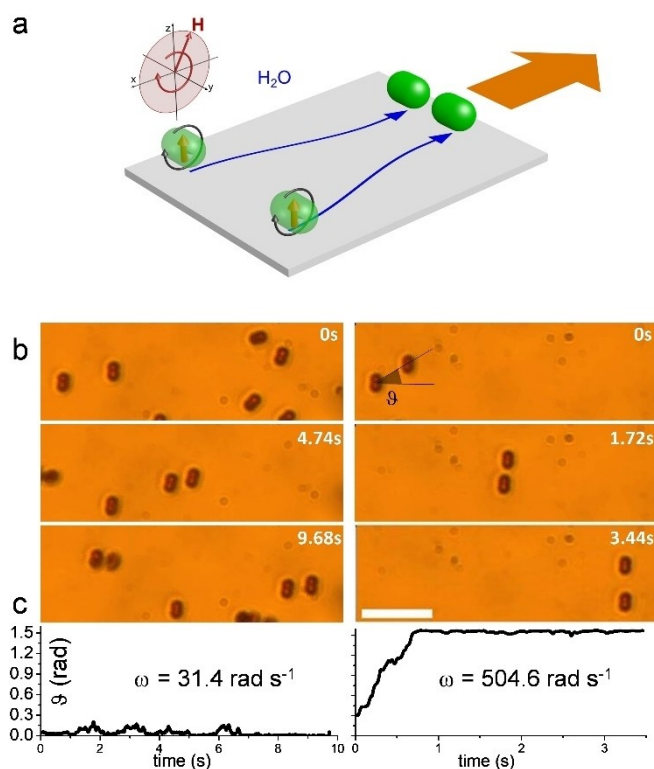
Figure 2. (a) Schematic of a pair of spinning hematite ellipsoids with a permanent moment, represented by the red arrows within the particles. The microrotors approach each other during propulsion. (b) Experimental images of the microellipsoids driven by a circular polarized rotating field with amplitude $H = 4400$ A m^{-1} and frequency $\omega = 188.5$ rad s^{-1} (left) and $\omega = 502.6$ rad s^{-1} (right). The scale bar is 10 μm. (c) The bottom panel shows the relative positional angle ϑ versus time. Reproduced with permissions from Ref. [28] (Copyright 2008, American Association for the Advancement of Science).

$F_m = 3\mu_m m^2/(4\pi r^4)$. The viscous force generated by a single propeller at an elevation h and spinning at a frequency Ω is, $F_v = 3\pi h^2 \eta \Omega/4$ being $\eta = 10^{-3}$ Pa·s the viscosity of the medium, here water. For a close distance of the order of the particle diameter, $r \sim 2h \sim 1.4$ μm, one find that $F_v/F_m = 0.02\ \Omega$ that leads to prevalence of magnetic interaction at low frequencies ($F_v = 0.6F_m$ for $\Omega = 31.4$ rad s^{-1}) and of hydrodynamics at large one ($F_v = 9.1F_m$ for $\Omega = 504.6$ rad s^{-1}). Such argument, however, does not capture the complexity of this state. In the high frequency regime, the particles are observed to adjust their velocity so that they to couple their vortical flow field. A numerical simulation study reveals the complex tip dynamics, not appreciable by the experiments, where the two ellipsoids in the bound state perform small relative orbital motions.[28]

When considering several spinning rotors, Michelle Driscoll et al. showed that hydrodynamic interactions lead to a new type of instability.[29] The magnetic rollers in this study have a relative weak dipolar coupling, and thus interact mainly by their generated fluid flow. The authors observe that the particles self-organize into motile structures as large-scale rolling swirls. Increasing the density of the microrollers give rise to a series of interesting phenomena, including a raise of the collective

translational speed, and the formation of shock waves,[30] similar to driven bubbles in microfluidc systems.[31] Later, when considering pair of such microrollers, Delmotte[32] demonstrated that they can exhibit hydrodynamic bound states where the particles couple along the third dimension producing a leap-frog type of motion. Such dynamic state has been simultaneously reported in experiments by Massana et al. with the hematite particles.[33]

2.3. Ferromagnetic rollers

Steady rotation of magnetic colloidal spheres could also be realized by a single axis excitation in the case of ferromagnetically ordered particles.[34] In contrast to paramagnetic particles, ferromagnetic spheres keep their magnetic moment even in the absence of the external magnetic field.

The presence of a permanent magnetic moment allows the use of different mechanism of particle actuation leading to spinning: instead of multiaxial fields (rotational or precessing) a single axis oscillating field can be employed. The external AC field is usually applied perpendicular to the surface supporting the particles, $H(t) = H_0 \sin(2\pi f)e_z$, to avoid any preferred direction along the surface, see Figure 3(a). The onset of a steady rotation and subsequent rolling of a spherical ferromagnetic particle is associated with a spontaneous symmetry breaking of the clockwise/counter clockwise particle oscillations observed in a certain range of the magnetic field parameters.[34,35] The steady spinning of particles is realized when the following condition is satisfied:
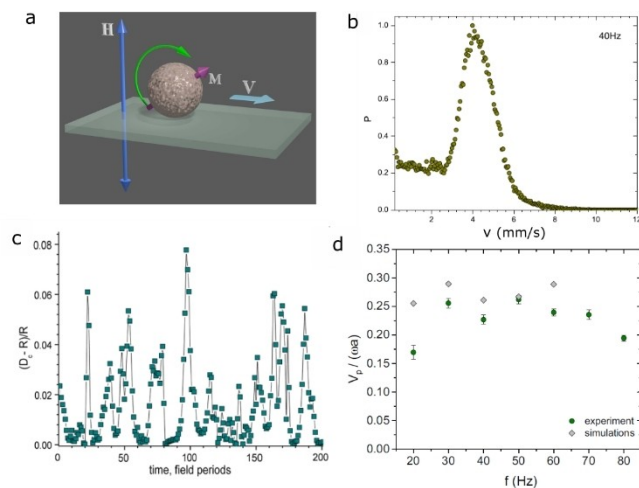
Figure 3. (a) A sketch of a uniaxial oscillating magnetic field excitation of a ferromagnetic colloidal sphere. Steady particle rotation leads to a self-propulsion with the velocity V along a direction not prescribed by the applied field. (b) Ferromagnetic rollers velocity distribution function. Instantaneous velocity values of individual rollers are taken at $f = 40$ Hz. Reproduced with permissions from Ref. [34] (Copyright 2017, American Association for the Advancement of Science). (c) Trajectory of the centre of mass of a roller versus time. D_c stands for the distance of the roller centre of mass from the rolling surface. (d) Ratio between the peak velocity and the no-slip particle velocity $V_0 = \omega R$. Reproduced with permissions from Ref. [35] (Copyright 2019, American Physical Society).

$$Im(\nu[-p^2, 2q]) - p > 0 \qquad (4)$$

Here, parameters $p = \alpha_r/(\omega I)$ and $q = \mu B_0/(\omega^2 I)$, where $\omega = 2\pi f$, η is the fluid's dynamic viscosity, and μ, m, $I = 2/5\, mR^2$, $\alpha_r = 8\pi\eta R^3$ are correspondingly the magnetic moment, mass, moment of inertia and the rotational drag coefficient of a roller. ν is the Mathieu characteristic exponent function. In the state of a steady rotation, the magnetic torque on the particle, $T_m = \|\mu \times B\|$, is balanced by its viscous torque, $T_v = \alpha_r\omega$. A similar, more robust steady rotation can also be a result of a particle shape anisotropy, if such anisotropic particle sediment with an orientation that is not aligned with the magnetization.[36] Particle inertia plays a key role in the emergence of a spinning motion of a magnetic sphere in a uniaxial field, and it constitutes an important distinction of this system from other torque-driven particles such as Quincke rollers or particles energized by rotating fields, as the magnetic rotors of previous section. Magnetic rollers rotate in synchrony with the periodic change in the direction of the alternating magnetic field, and the speed of their rolling motion is determined by the field frequency. Since the single-axis field excitations are perpendicular to the substrate, the actuation mechanism does not prescribe the direction of particle rolling motion, and each particle spontaneously selects the direction of propulsion once the system is energized. Although individual particles roll and exhibit self-propelled motion, the particle velocity distribution is often broad due to shape imperfections of individual particles (as illustrated in Figure 3(b)). The size of the particles used in the experiments is of the order of 100 μm.

It has been reported experimentally and captured by simulations[34,35] that the speed of rolling does not match to the expected speed calculated for the case of no-slip conditions at the interface. In the limit of no-slip contact with the surface, the rolling speed V_0 would be $V_0 = \omega\, R$, where $\omega = 2\pi f$. However, the experiments indicate that this theoretical speed value is not attainable (see Figure 3). The particle rolling speeds are distributed around mean value V, which is of the order $V \approx 0.2$–$0.3\, V_0$ in the whole frequency range used in the experiments. Two main factors contribute to the speed reduction. First, the fluid works as a lubricant, leading to partial slip between the particle and the bottom, and second, a moving rotating particle near a solid surface experience a lift force, which is of the order of the gravitational force. In the Stokes limit, the lift force on a rotating sphere is $F_L = \pi\rho_f R^3 \omega\, V$, where ρ_f is the fluid density, and V is the particle translation velocity. When the lift force dominates the gravitational force, the rolling colloids have an upward motion. As a result, when in the vicinity of other rollers creating anisotropic hydrodynamic flows, the motion of a typical ferromagnetic roller experience frequent departures and returns from the rolling surface as demonstrated by a typical trajectory of the centre of mass of a ferromagnetic roller illustrated in Figure 3(c).

Once in motion, a gas of ferromagnetic rollers demonstrates a normal (Fickian) diffusion with a characteristic linear growth of the mean-squared displacement. Nevertheless, the statistics of displacements stay non-Gaussian: at short times the system has a bimodal distribution of the displacements that transit with time to a quasi-Gaussian distribution.[36]

3. Assembly of spherical rotors

3.1. One-dimensional systems: microworms

External magnetic fields can be used to induce a net attractive interaction between propelling rotors and condense the dispersed particles into elongated structures. The example in Figure 4(a) shows the formation of a propelling colloidal "worm" made of paramagnetic particles.[37] The constituent units are commercially available spherical paramagnetic colloids, here polystyrene particles doped with nanoscale iron oxide grains. In principle the rotating field cannot apply a torque to these particles since they are not ferromagnetic, anisotropic (such as the DNA linked doublets) or present any built-in magnetic anisotropy. Under an external field H a paramagnetic particle of volume V acquires an induced moment $m = V\chi H$ pointing along the field direction. Here χ denotes the magnetic volume susceptibility of the particle. Thus, in an ideal case, when the field rotates, such moment will rotate within the particle and $T_m = 0$. However, as shown in Figure 4(b), experiments demonstrate that individual particles display a small but non negligible drift and thus, can be effectively spin by the rotating field.

The reason is that such paramagnetic colloids present a finite internal relaxation time of the magnetization.[38] This relaxation enables a non-zero magnetic torque when averaged over many field cycles, $T_m = \mu_m \langle m \times H \rangle$. Thus, the particles acquire an angular speed in general lower than the driving one, $\Omega < \omega$.

The colloidal worm is created by a strongly elliptical polarized field, $\beta \sim 0.5$, so that $H_x \gg H_z$. Such field induces time-average attractive dipolar interactions which assemble the
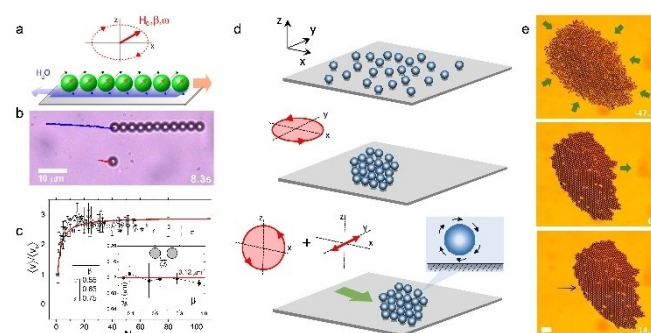

Figure 4. (a) An ensemble of paramagnetic microrotors assembled and driven by an elliptically polarized rotating field. (b) Microscope image of a chain (the trajectory is superimposed in blue) and of an individual particle (in red) after 8.3 s of propulsion. (c) Normalized speed versus number of particles in the chain. Reproduced with permissions from Ref. [37] (Copyright 2015, American Physical Society). (d) Schematic illustrating the assembly and propulsion of a two-dimensional carpet made of paramagnetic microrotors. (e) Corresponding experimental images of the propelling carpet. Scale bar at the bottom is 20 μm. Reproduced with permissions from Ref. [40] (Copyright 2019, Nature Publishing Group).

particles into elongated chains. When averaging Eq. (3), the dipolar potential becomes attractive along the propulsion direction, here the $x-$axis, $\langle U_{dd} \rangle = -(\mu_m m^2/8\pi(x+z)^3)$. In contrast $\langle U_{dd} \rangle$ is repulsive along the perpendicular direction ($y-$axis), which explains why these trains do not combine into two dimensional sheets. Further, as shown in Figure 4(c) chains of rotors propel faster than individual particles, and the average speed rapidly raises with N reaching a saturation value around a length of $N \sim 30$ particles. This "speed up" effect originates from the cooperative flow field of the rotating particles. The flow continuously advects the colloidal chain like a hydro-dynamic conveyor belt, and it creates two shear zones with opposite directions, one on top of the chain and the other in the space between the chain and the close surface. The flow additivity raises the average speed of the chain. However, beyond a given length the rotors are too far, and such flow additivity becomes negligible.[37] This hydrodynamic "conveyor belt" allows non-magnetic tracer particles to be trapped and translated on top of the chain at a faster speed. Thus, it could be used as an efficient method to transport and shuttle drugs without directly attaching them to the particles, a similar case is described in Section 5.

3.2. Two-dimensional sheets of rotors: carpets

The previous one-dimensional structure could be extended into two-dimensions by using a more complex magnetic modula-tion. This effect was demonstrated by Martinez-Pedrero *et al.*[39] and its principle is shown in Figure 4(d). Starting from the dispersed particles, one first need to create a two-dimensional compact cluster by using attractive dipolar interactions. These interactions are induced with an in-plane (x, y) rotating magnetic field.[41] After that, the cluster is transformed in a carpet of rotors by switching immediately to a field that performs circular rotations in the perpendicular plane, here the (x, z). An additional component oscillating along the y-direction is then superimposed to the magnetic modulation to keep the structure stable, i.e. avoid lateral separation into parallel chains. The modulation is now able to torque the particles, but at the same time it keeps the structure stable, as long as the additional oscillating field is kept on.

This dynamically assembled structure demonstrates differ-ent interesting features. First, it allows microscopic cargos to be transported above its extended region as budding yeast cells (Saccharomyces Cerevisiae) or silica-dioxide microspheres.[39] Further, as shown in Figures 5(a,b), it features self-healing.[40] This is observed when increasing the amplitude of the out of plane component (H_z) of the rotating field. Above a threshold value, the driving field induces a tread-milling like motion above the carpet. Particles located at the back detach from there, translate above the carpet by its conveyor belt, and finally reattach in front of it. This effect generates a continuous colloidal flow that can regenerate the structure. If the carpet initially presents defects in form of holes, the particles reach these holes and fill them by recovering the entire structure. Even in the presence of grain boundaries, the carpet can be
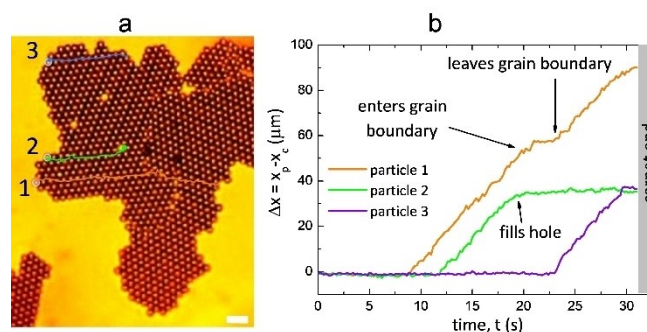
Figure 5. (a) A carpet of magnetic microrotors with the trajectories of three particles that have been detached from the back due to the tread-milling effect. Scale bar is 20 μm. (b) Position versus time of the particles to illustrate the three possible situations: 1) a particle that enters and leaves a grain boundary, 2) a particle that fills a hole and 3) a particle that reaches the edge of the carpet. Reproduced with permissions from Ref. [40] (Copyright 2019, Nature Publishing Group).

continuously grown in a defect-free structure by this colloidal flow after few seconds of propulsion.

3.3. Dynamic assembly of ferromagnetic rollers

Magnetic colloidal rollers introduced in Section 2.3 demonstrate a strong propensity toward the onset of a large-scale collective motion. A set of dynamic phases ranging from gas to intermittent linearly translating flocks, and the emergence of a global vortex has been observed in the harmonically confined (soft harmonic gravitational confinement) ensembles of ferro-magnetic rollers in response to changes in the rollers' activity controlled by the frequency of the uniaxial field.[34] The particles sediment on a concave bottom surface of a liquid-filled container. The emergence of collective states is attributed to the development of velocity correlations between the rollers promoted by long-range hydrodynamic and magnetic interactions.[34,35]

Transitions between dynamic self-organized states are often quantified by the corresponding order parameter, ϕ_R, defined as

$$\phi_R = \frac{1}{N} \sum_{i=1}^{N} \mathbf{e}_{\varphi i}(t) \mathbf{v}_i(t) \tag{5}$$

Here $\mathbf{e}_{\varphi i}$ are in-plane unit vectors in angular direction, and $\mathbf{v}_i$ are in-plane unit velocities of the individual rollers. At low frequencies ($f < 30$ Hz) a gas state of randomly moving rollers is observed with a corresponding order parameter close to zero. The velocities of the individual rollers are uncorrelated. An increase in the frequency of the driving field leads to the onset of a collective behaviour reminiscent of bird flocks, where large groups of rollers start to move coherently for a prolonged amount of time. The correlations in particles' motion translate into a growth of the order parameter, see Figure 6(a,b). Further increase in the activity results in the growth in size and
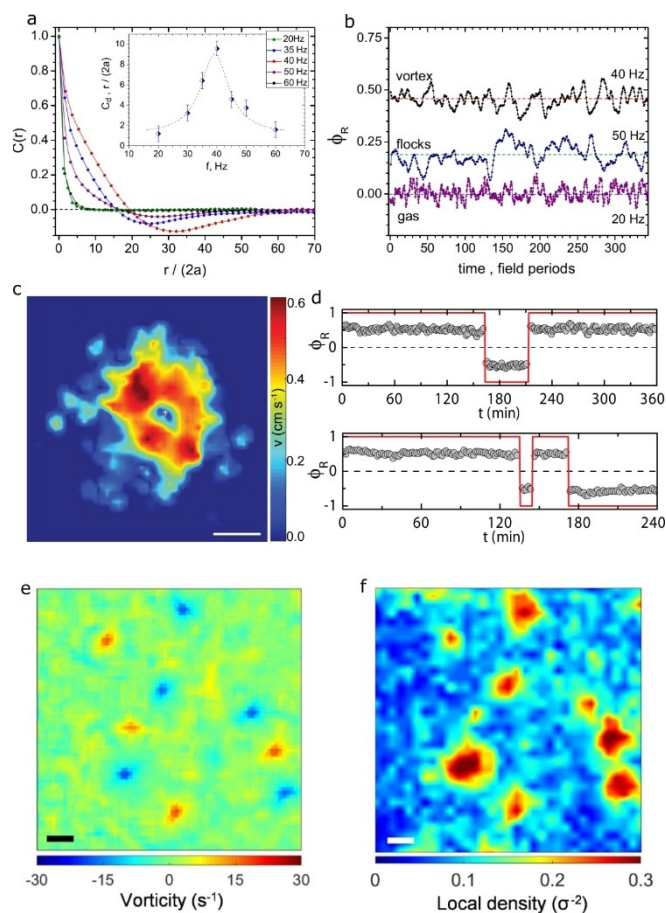
Figure 6. (a) Spatial particle velocity correlation function at different excitation frequencies of the uniaxial driving magnetic field. Insert: corresponding correlation length as a function of frequency. (b) order parameter ϕ_R for typical dynamic states: gas, vortex, flocks. Reproduced with permissions from Ref. [34] (Copyright 2017, American Association for the Advancement of Science). (c) Velocity amplitude field of a self-organized roller vortex. Scale bar is 2 mm. (d) Vortex chirality switching events illustrated by the polar order parameter. $B_0 = 5.78$ mT, $f = 40$ Hz. Reproduced with permissions from Ref. [42] (Copyright 2018, Nature Publishing Group). (e) Vorticity field of the rollers in a state with spontaneous multiple vortices extracted from particle image velocimetry. (f) Local roller number density map demonstrating dynamic densifications at locations of vortices. Scale bar is 5 mm. Reproduced with permissions from Ref. [44] (Copyright 2020, the National Academy of Sciences of the USA).

persistence time of the flocks, and eventually leads to the emergence of a vortex spanning the entire system, see Figure 6(c). The velocity correlations in the vortex state reach maximum, and the corresponding order parameter attains its highest value. The sense of rotation is spontaneously selected by the system and changes from experiment to experiment. Further increase in the frequency results in the breakdown of the coherent vortex motion and formation of re-entrant flocks and, finally, a gas-like state (see insert in Figure 6(a)).

All dynamic states in the ensemble of ferromagnetic rollers are reversible with the frequency of the energizing magnetic field. It was subsequently demonstrated that emergent roller vortices can spontaneously change the sense of rotation.[42] In Figure 6(d) the chirality switching events are illustrated as they

manifest in the polar order parameter of a roller vortex formed in a soft harmonic gravitational confinement. The vortex chirality switching is stochastic and relatively rare event on the scale of a typical experiment. It was demonstrated that the spontaneous chirality switching proceeds through the intermittent formation of flocks. During this intermittent process, the rollers again randomly select a new chirality state that also can result in instances where vortex falls back to its previous chiral state.[42]

Additionally, a method not relying on harmonic confinement for guided self-assembly and control of self-organized colloidal roller vortices was realized.[43] It was shown that the structure of a vortex composed of rolling magnetic particles can be stabilized and effectively manipulated by means of an additional strongly localized alternating magnetic field provided by a mini-coil (about 4 mm radius) aligned collinear with the main coil and operating at the same frequency. By tuning the parameters of the localized field (phase and amplitude) that constituted a fraction of the driving field, the dimension and particle number density in the vortex could be controlled.[43] The roller vortex self-organization is assisted by field-induced magnetic "steering" rather than magnetic field gradients and is only possible while the system is in the active (magnetic rollers) state. In addition, parameters of the emergent vortex (size and density) are efficiently tuned by a phase shift between the alternating magnetic fields.[43]

It was recently demonstrated that the emergence of dynamic roller vortices can spontaneously form in an open (unconfined) environment.[44] The novel states are characterized by multiple emergent vortices with complex spatiotemporal dynamics where vortices can appear, translate and disintegrate far from the boundaries, see Figure 6(e,f). The vortices are stable and preserve their shape for a long time, while constantly exchanging roller material with their neighbours. The coexistence of vortices and flocks has been reported in this system. Clockwise and counter-clockwise vortices are simultaneously present in the system with equal probability. In both experiments and modelling, vortices have the nearest neighbourhood with predominantly opposite chiralities,[44] see Figure 6(e). The apparent quasi-antiferromagnetic ordering of the vortices prevents viscous shear stress accumulation in the system. The formation of roller vortices not associated with any confinement is driven by spontaneous local densifications in the ensemble, see Figure 6(f). The core of each vortex exhibits a solid body-like rotation with nearly uniform density, and the characteristic size of the vortex is determined by the coherence length $\xi \sim \sqrt{2\pi f \tau_{dif}/\rho}$ of the system.[44] Here, ρ is the number density in the vortex core, and τ_{dif} is a characteristic diffusion time. The emergent vortices are mobile, can travel long distances, and capture passive particles in their cores.[42]

The onset of long-range coherence in the system of magnetic rollers also accompanied by a spontaneous phase synchronization between different rollers forming a vortex.[34,35] Since each roller is also synchronized with the phase of the vertical uniaxial field, global control of the collective motion with the phase of the driving field becomes possible. In this way once formed a confined roller vortex can be prescribed a

chirality by a temporal modulation of the driving field phase.[45] This approach has been successfully realized in controlling chiral states of a spontaneous magnetic roller vortex in a confining droplet. It was possible to systematically change the chiral state of a self-assembled vortex on-demand in a uniaxial vertical field,[45] see Figure 7.

4. Collective phases in spinner materials

Most of the review so far has been focused on self-locomoting magnetic particles (with translational activity). In this section we review the magnetic colloidal systems with activities originating from pure rotational motion without self-propulsion. One of the first realizations of dynamically assembling magnetic spinners has been demonstrated at the macroscopic level in a system of magnetized disks suspended at a liquid interface and powered by a rotating magnetic field.[49] It has been demonstrated that a same-wise rotation of particles leads to stable dynamically ordered phases similar to crystals.

4.1. Self-assembled magnetic spinners

Recently developed approaches exploiting dynamic self-assembly of magnetic colloidal particles provide a robust method for generating large ensembles of microscopic spinners.[46–48] It has been demonstrated that the application of a uniaxial external

magnetic field oscillating in-plane of the interface supporting ferromagnetic spherical particles can lead to multiple self-assembled spinners with a narrow size distribution, see Figure 8.

Interfacial spinners generated by a uniaxial alternating magnetic field (see Figure 8(a)) emerge as a result of spontaneous symmetry breaking of clock/counterclockwise rotations experienced by self-assembled chains of ferromagnetic particles in a certain range of the driving magnetic field parameters.[46] Dynamic spinners are composed of short self-assembled chains of micro-particles ferromagnetically ordered due to the prevailing magnetic dipole-dipole inter-particle interactions. Spinners rotate clockwise (CW) or counterclockwise (CCW) with the frequency of the applied field.

The onset of spinning is related to the following mechanism. The applied AC magnetic field forces the chain to align with the field orientation, resulting in periodic (with the field frequency) reversals of the direction. If the chain's rotational inertia is large compared to the viscous drag, the chain will preferably rotate in one of the directions. The length of a spinner is determined by a balance between magnetic and viscous torques acting on a chain at the liquid interface. Balancing the torques, one finds (in the slender body approximation) that $L_s^2/\log(L_s/R) \sim A/\omega$. Here, L_s is a characteristic spinner length, R is a radius of microparticles, and A is a factor that depends on magnetic moment of the particles, their radius, the amplitude of the applied magnetic field and the viscosity of
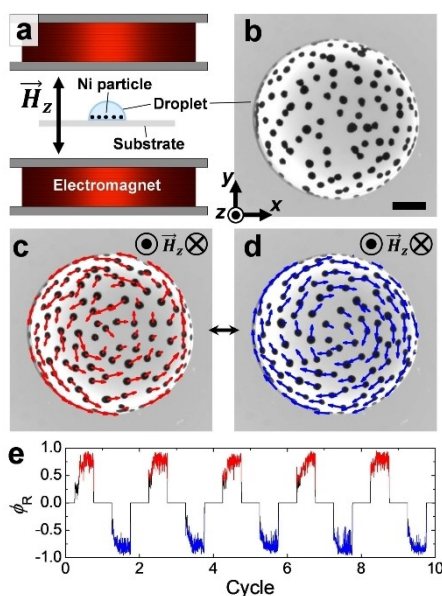
Figure 7. (a) Schematic illustration of the experimental setup. (b) A snapshot of a dispersion of the Ni particles confined inside a water droplet. The scale bar is 0.5 mm. (c) and (d) An emergent roller vortex. The self-organized magnetic rollers exhibit right- (c) and left-handed (d) vortical motion in which the arrows indicate the actual moving direction of the rollers. A phase shift δ = π in the sinusoidal magnetic field allows the reversible transition between the (c) and (d) states. (e) The time evolution of the mean polar order parameter in the vortex, ϕ_R, for 10 discrete cycles of the chirality manipulation. Reproduced with permissions from Ref. [45] (Copyright 2021, The Royal Society of Chemistry).
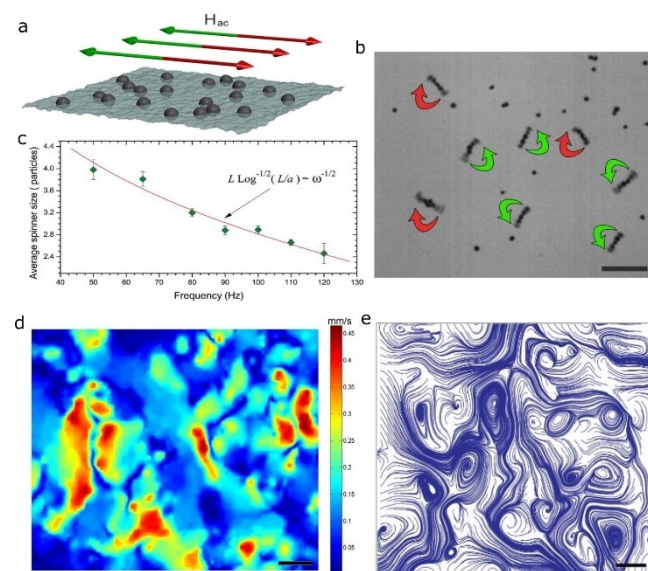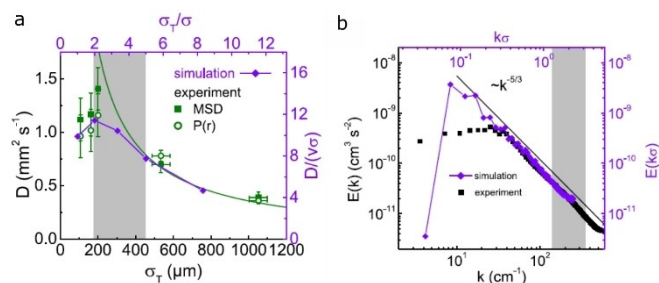

Figure 8. (a) Schematics of the uni-axial excitation of ferromagnetic ensemble suspended at a liquid interface. Oscillating magnetic field is applied parallel to the liquid surface. (b) a snapshot of a spinner phase formed at f = 50 Hz, B_0 = 2.9 mT. Short chains of particles rotate in either direction with the frequency of the applied magnetic field. Clock- and counter-clock-wise spinners are illustrated by arrows. Scale bar is 1 mm. (c) a characteristic spinner size versus driving field frequency. (d) An experimental snapshot of a hydrodynamic velocity field in spinner ensemble. (e) A typical streamline pattern of hydrodynamic surface flows. Scale bar is 2 mm. Reproduced with permissions from Ref. [46] (Copyright 2015, Nature Publishing Group).

the media,[46] see Figure 8(c). Both flavours (CW and CCW) spinners are equally probable and simultaneously present in the system (Figure 8(b)). The spinners inject the energy by a torque transfer via the generation of local vortex flows. The energy injection rate and the corresponding injection scale can be tuned by the frequency and amplitude of the applied magnetic field. While spinners are not self-propelling entities, they are advected by induced flows of neighbouring spinners. Erratic motion of spinners by advection flows result in a turbulent-like appearance of 2D velocity field, see Figure 8(d,e).

Transport characteristics of such spinner liquids are not trivial. The active diffusion (diffusive motion of passive particles promoted by the activity of the spinner sub-system) increases linearly with the spinner density and is approximately independent of the frequency of the driving field.[48] Moreover, it was demonstrated that the dependence of the active diffusion coefficient on the inert particle size is non-monotonic. The Stokes-Einstein relation, $D \sim 1/\sigma_{T,}$ (here σ_T corresponds to a characteristic tracer size) holds for large inert particles (larger than a spinner) and diffusion is suppressed for small particles, see Figure 9(a). At elevated concentrations, the system of ferromagnetic spinners develops dynamic segregation and clustering of spinners with the same sense of rotation.[47]

A typical energy spectrum $E(k)$ of self-induced interfacial flows generated in spinner ensembles resembles that of an inverse energy cascade in 2D turbulence. The broad energy-injection scale (shown as grey area in Figure 9(b)) arises from a spinner-size heterogeneity. A characteristic power-law behaviour can be clearly observed over more than an order of magnitude in length scale.[47] The power-law decay with a characteristic exponent $k=-5/3$ of the energy spectrum corresponds to that typically found in a high-Reynolds number turbulence, while Re is only about 30 for the flow-generating spinners in the spinner system.

In a related work[50] the collective motion of a square array of fixed magnetic rotors actuated by an external magnetic field which osci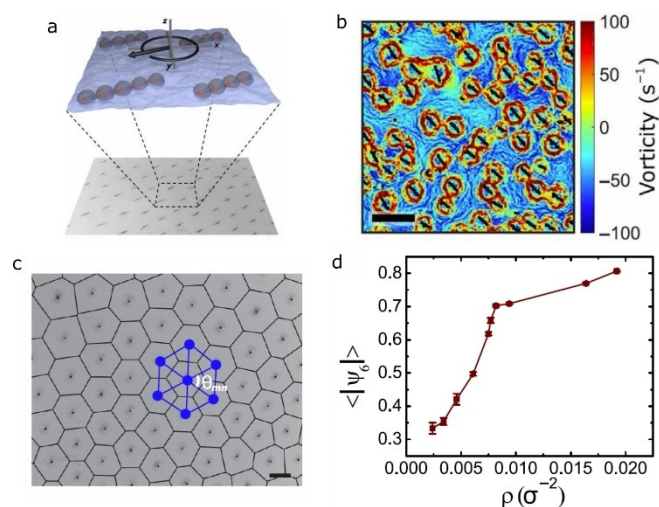llated along one axis of the array was investigated. By changing the relative strength of the external field and the dipolar interactions between the rotors, different collective rotational patterns have been observed. In the case of the dominant dipole interaction the rotors oscillated back and forth, clockwise or counter-clockwise in alternating stripes. In the case of the external field dominance, the magnetic rotors underwent full rotations with different quadrants of the array turning in different directions.[50] These collective modes of rotation can be utilized for mixing or pumping fluid.

4.2. Synchronized magnetic spinner liquids

A related system to the one described in the previous paragraph is composed of synchronized self-assembled spinners. This kind of spinners with externally imposed synchronization can be realized by the application of an in-plane rotational magnetic field instead of an oscillating uniaxial one.[48] Similar to the previous case, the rotational magnetic field promotes the dynamic self-assembly of the ferromagnetic particles into multi-particle linear chains with a characteristic length determined by the same balance between magnetic and viscous torques discussed above. However, now all self-assembled chains remain synchronized with the rotation of the external field, see Figure 10. Self-assembled spinners locally inject vorticity into the liquid interface and generate strong hydrodynamic flows, leading to a set of collective dynamic phases and promoting active diffusion. Transitions from a spinner liquid phase to stable two-dimensional (2D) dynamic crystalline lattices (illustrated by a snapshot of the lattice in Figure 10(c) and the

Figure 9. (a) The active diffusion coefficient is a nonmonotonic function of the inert particle size for experiments (green; f = 60 Hz) and simulations (violet). The green line indicates the dependence D ~ 1/σ_T. The grey area corresponds to the range of spinner sizes. (b) Energy spectrum E(k) of the surface flows as obtained from experiments (black) and simulations (violet). 2D turbulent flow reverse energy cascade toward small wave numbers k with k = −5/3 scaling. The energy injection region is shown in grey. The experimental parameters: B₀ = 2.7 mT, f = 60 Hz. Reproduced with permissions from Ref. [47] (Copyright 2017, the National Academy of Sciences of the USA).

Figure 10. (a) Ensemble of spinners under influence of a rotational magnetic field applied in-plane of the interface supporting ferromagnetic particles. (b) vorticity field of the flows induced by synchronized spinners. f = 90 Hz. Scale bar is 1 mm. (c) A dynamic lattice formed from spinners at f = 45 Hz. Voronoi diagram is overlaid with the experimental lattice. The spinners are blurred because of the long exposure time that enabled precise identification of the rotational axes for all spinners. Scale bar is 1 mm. (d) The mean |Ψ₆| value of the spinner lattices illustrates the liquid-to-crystalline dynamic transition with the spinner density. Reproduced with permissions from Ref. [48] (Copyright 2020, American Association for the Advancement of Science).
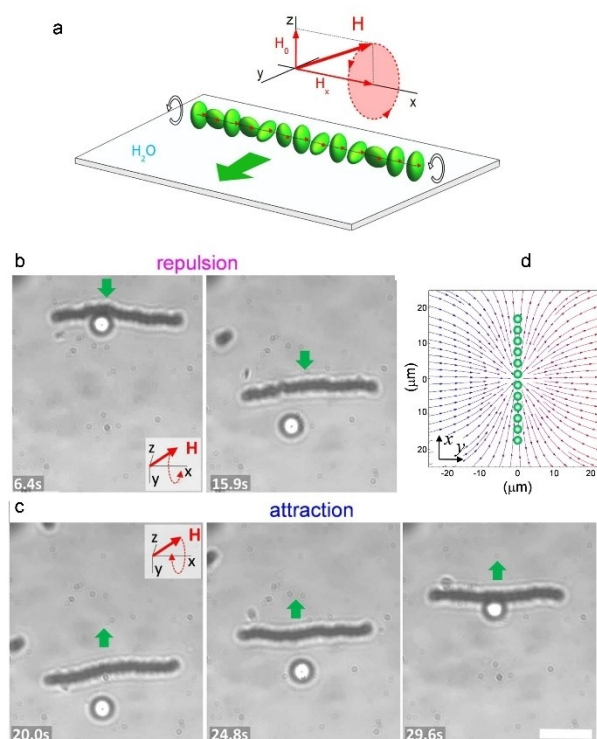
behaviour of the hexagonal bond orientational order shown in Figure 10(d)) are driven by the increasing spinner density.[48]

The lattices of synchronized spinners give rise to a new class of active crystals accompanied by a vigorous vortical flow field. The system of synchronized spinners is intrinsically out of equilibrium, and the structure is maintained only while the continuous external energy input is present.[49,50] Being active by nature, self-organized spinner lattices exhibit self-healing behaviour: a spinner lattice damaged by external mechanical intrusion is quickly filled with newly assembled spinners and the order is restored.[48]

Synchronized spinner lattices support strong self-induced underlying hydrodynamic flows, a lattice of such spinners is able to effectively facilitate the transport of passive cargo particles. Active diffusion coefficient values in the range of 1 to 7 mm^2/s are orders of magnitude higher than those corresponding to thermal Brownian diffusion. The active diffusion coefficient in active spinner materials can be efficiently tuned by the parameters of the external energizing field. It was demonstrated that for relatively large passive particles (approaching the size of the spinners) active diffusion can be substantially manipulated by the external field frequency: the diffusion coefficient linearly decreases with the frequency increase. This unconventional behaviour is attributed to the changes in the characteristic spinner-spinner distances within the lattice, leading to a "caging" effect experienced by a cargo bead when shrinkage of the spinner lattice unit cell coupled with faster induced flows (due to faster spinner rotations) makes it more difficult for a passive particle to leave the lattice cell.

Figure 11. (a) Sketch of a magnetic ribbon made of 13 hematite particles assembled and propelled by a magnetic field performing a conical precession along the x-plane. (b,c) Microscope images illustrating the interaction via repulsion (b) and attraction (c) due to hydrodynamic flow with a silica particle (diameter 4 μm). (d) Streamplot of the flow field generated by a chain of propellers that translate from left to right. Colours correspond to incoming (blue) and outcoming (magenta) flows. (a–d) Reproduced with permissions from Ref. [55] (Copyright 2017, IOP Institute of Physics).

5. Mixed and hybrid systems

We now comment on two recent trends in the field: 1) mixing passive particles with active propelling rotors and, 2) developing hybrid systems based on complementary actuation schemes. In the first case, non-magnetic particles are often used as passive tracers to visualize the hydrodynamic fluid flow generated by the magnetic rotors. The principle is similar to particle image velocimetry,[51] and it determines the flow streamlines from the tracking of the tracer particles. The same flow produced by a moving rotor can be used to trap a passive cargo, and transport it in a controlled way. The latter effect is usually demonstrated by relatively large non-magnetic spheres, to avoid the particle escape along the third dimension induced by thermal fluctuations. The hydrodynamic trapping effect with a surface propeller was demonstrated by Zhang *et al.* with a rotating Ni-nanorod,[15] although earlier work with microfluid pumps[52] and with magnetic thin films[53] already showed the possibility of using backflow currents to drag micro-spheres. Subsequent theoretical work has shown that the hydrodynamic trapping is accomplished through time irreversible interactions that force the cargo migration through the flow streamlines generated by the roller.[54] Another example of this capability has been demonstrated by H. Massana-Cid *et al.*[55] and is reported in Figure 11. In such work the authors generate a magnetic ribbon composed of a chain of ferromagnetic hematite particles. The ribbon is assembled and propelled by an external precessing field (Eq. 2), see Figure 11(a). A similar strategy has been used with paramagnetic colloidal chains by Casic *et al.*,[56] and in both cases the propulsion is perpendicular to the ribbon long axis. The ribbon is composed by several surface rotors and the generated hydrodynamic flow field trap and transport silica particles with 4 μm diameter, Figure 11(b,c). These particles could be either repelled (Figure 11(b)) or attracted (Figure 11(c)) when located in front or behind the propelling chain, respectively. However, the trapping mechanism becomes less efficient when using shorter ribbon, i.e. composed of only a few rotors, due to the edge effects and the corresponding reduction of the global flow.

As shown in Figure 11(d), the flow profile calculated numerically agreed with the experimental observation: is attractive behind the propelling ribbon (blue arrows) and becomes repulsive in front of the ribbon (magenta arrows). Further, the analysis of the streamlines show that the flow converges toward the ribbon center, thus forcing particles located close to the edge to migrate toward its center.

Regarding the use of hybrid actuation schemes, there are several examples in the literature where magnetic driving is

combined with another propulsion scheme, such as a chemical reaction,[57] ultrasound[58] or electric[59] fields, or other types of actuation. In general, combining these schemes could give rise to a higher level of functionality. For example, let us consider a combination of a chemical reaction with the magnetic actuation induced by a rotating field, Eq. (1), as explored in Ref. [60]. There the authors used a chemical reaction, namely the photoinduced decomposition of hydrogen peroxide (H_2O_2) in water, to induce the phoretic attraction of a small cargo to a hematite particle. The latter could be then moved in a fluid by the rotating field, that did not affect the attached cargo and represent an independent transport mean for the composite pair. The rotating field could also be used to vary the relative position of a carrier and cargo, or to change on demand a towing scheme from pusher to puller. Moreover, the ability to tune the speed of the prototype carrier with the frequency of the driving field allows precise control of cargo in a fluidic based microdevice. Alternatively, the magnetic prototype could be actuated by a chemical reaction, if the latter guarantees a faster transportation mechanism, and an external field can be used either to steer[61] or to assemble a series of micromotors.[62] Magnetic fields can also be used as complementary means of transport when catalysts are fully consumed.

6. Conclusion and future perspectives

We have presented an overview of recent experimental developments on magnetically driven particles propelling and self-assembling close to an interface. The presence of a bounding plane allows these particles to be confined in two-dimensions, a feature that simplifies their experimental observation which in most of the cases is made via optical microscopy. With precise particle tracking[63] one can extract the positions of the particles and directly measure their speed, orientations, or other properties of interest. The complex collective dynamics of magnetic surface rotors originate from the delicate balance between different forces, ultimately governed by magnetic and hydrodynamic interactions. The parameters of the applied magnetic field can be externally tuned to control these interactions, promote specific collective behaviour, and shed light on the role that different interactions play in the dynamic behaviour of these out-of-equilibrium colloidal ensembles.

Apart from the fundamental insights into emergent dynamics of magnetic colloids, there are numerous potential technological applications of surface magnetic rotors. Since these particles can be controlled and steered by an external field, they can be used as non-invasive drug delivery vectors to mix fluids, pick-up, transport and release microscopic cargos. In microfluidics, the basic operations are usually performed by mixing different streams of fluids and by allowing them to react within serpentine or elongated channels.[64,65] Equivalent procedures can be realized at the colloidal length-scale but without the need of hard wall confinements or physical constraints that often involve complex lithographic procedures. Thus, these features make surface rotors also attractive for applications in biotechnology and biomedical systems. Further possible appli-

cations of surface magnetic rotors and spinners include their use as very sensitive tribotatic detectors,[66] cargo transporters,[67] omnidirectional swimmers,[68] and topotactic magnetic rollers,[69] to cite a few of them.

Conflict of Interest

The authors declare no conflict of interest.

Keywords: Colloids · Magnetism · Active systems · Hydrodynamics

[1] P. M. Chaikin, T. C. Lubensky, *Principles of Condensed Matter Physics* **1995**, Cambridge University Press.
[2] A. Yethiraj, A. van Blaaderen, *Nature* **2003**, *421*, 513.
[3] A. Ashkin, *Phys. Rev. Lett.* **1970**, *24*, 156.
[4] A. T. Skjeltorp, *Phys. Rev. Lett.* **1983**, *51*, 2306.
[5] K. Zahn, G. Maret, *Phys. Rev. Lett.* **2000**, *85*, 3656.
[6] C. Bechinger, R. Di Leonardo, H. Löwen, C. Reichhardt, G. Volpe, G. Volpe, *Rev. Mod. Phys.* **2016**, *88*, 045006.
[7] a) H. Löwen, *J. Phys. Condens. Matter* **2008**, *20*, 404201; b) J. E. Martin, A. Snezhko, *Rep. Prog. Phys.* **2013**, *76*, 126601; c) J. Dobnikar, A. Snezhko, A. Yethiraj, *Soft Matter* **2013**, *9*, 3693; d) S. H. L. Klapp, *Curr. Opin. Colloid Interface Sci.* **2016**, *21*, 76.
[8] a) A. Najafi, R. Golestanian, *J. Phys. Condens. Matter* **2005**, *17*, S1203; b) E. Lauga, T. R. Powers, *Rep. Prog. Phys.* **2009**, *72*, 096601.
[9] E. M. Purcell, *Am. J. Phys.* **1977**, *45*, 3.
[10] R. Dreyfus, J. Baudry, M. L. Roper, M. Fermigier, H. A. Stone, J. Bibette, *Nature* **2005**, *437*, 862.
[11] a) F. Y. Ogrin, P. G. Petrov, C. P. Winlove, *Phys. Rev. Lett.* **2008**, *100*, 218102; b) L. Zhang, J. J. Abbott, L. Dong, K. E. Peyer, B. E. Kratochvil, H. Zhang, C. Bergeles, B. J. Nelson, *Nano Lett.* **2009**, *9*, 3663; c) A. Ghosh, P. Fischer, *Nano Lett.* **2009**, *9*, 2243; d) O. S. Pak, W. Gao, J. Wang, E. Lauga, *Soft Matter* **2011**, *7*, 8169.
[12] a) W. F. Paxton, K. C. Kistler, C. C. Olmeda, A. Sen, S. K. S. Angelo, Y. Cao, T. E. Mallouk, P. E. Lammert, V. H. Crespi, *J. Am. Chem. Soc.* **2004**, *126*, 13424; b) J. R. Howse, R. A. L. Jones, A. J. Ryan, T. Gough, R. Vafabakhsh, R. Golestanian, *Phys. Rev. Lett.* **2007**, *99*, 048102.
[13] A. Snezhko, *Curr. Opin. Colloid Interface Sci.* **2016**, *21*, 65–75.
[14] A. Snezhko, M. Belkin, I. S. Aranson, W. K. Kwok, *Phys. Rev. Lett.* **2009**, *102*, 118103.
[15] L. Zhang, T. Petit, Y. Lu, B. E. Kratochvil, K. E. Peyer, R. Pei, J. Lou, B. J. Nelson, *ACS Nano* **2010**, *4*, 6228.
[16] P. Tierno, R. Golestanian, I. Pagonabarraga, F. Sagués, *Phys. Rev. Lett.* **2008**, *101*, 218304.
[17] a) J. E. Martin, *Soft Matter* **2016**, *12*, 5636–5644; b) K. J. Solis, J. E. Martin, *Soft Matter* **2017**, *13*, 5676.
[18] J. Loehr, M. Loenne, A. Ernst, D. de Las Heras, T. M. Fischer, *Nat. Commun.* **2016**, *7*, 1–10.
[19] A. J. Goldman, R. G. Cox, H. Brenner, *Chem. Eng. Sci.* **1967**, *22*, 637.
[20] F. Martinez-Pedrero, H. Massana-Cid, P. Tierno, *Small* **2017**, *13*, 1603449.
[21] T. Sugimoto, M. M. Khan, M. Muramatsu, *Colloids Surf. A* **1993**, *70*, 167.
[22] F. Martinez-Pedrero, A. Cebers, P. Tierno, *Soft Matter* **2016**, *12*, 3688.
[23] C. G. Shull, W. A. Strauser, E. O. Wollan, *Phys. Rev.* **1951**, *83*, 333–345.

[24] A. Cebers, M. Ozols, *Phys. Rev. E* **2006**, *73*, 021505.

[25] P. Tierno, J. Claret, F. Sagués, A. Cebers, *Phys. Rev. E* **2009**, *79*, 021501.

[26] a) H. Morimoto, T. Ukai, Y. Nagaoka, N. Grobert, T. Maekawa, *Phys. Rev. E* **2008**, *78*, 021403; b) P. Tierno, R. Golestanian, I. Pagonabarraga, F. Sagués, *J. Phys. Chem. B* **2008**, *112*, 16525; c) C. E. Sing, L. Schmid, M. F. Schneider, T. Franke, A. Alexander-Katz, *Proc. Natl. Acad. Sci. USA* **2010**, *12*, 535–540; d) A. van Reenen, A. M. de Jong, M. W. J. Prins, *Lab Chip* **2015**, *15*, 2864.

[27] P. Tierno, O. Güell, F. Sagués, R. Golestanian, I. Pagonabarraga, *Phys. Rev. E* **2010**, *81*, 011402.

[28] F. Martinez-Pedrero, E. Navarro-Argemí, A. Ortiz-Ambriz, I. Pagonabarraga, P. Tierno, *Sci. Adv.* **2018**, *4*, eaap9379.

[29] M. Driscoll, B. Delmotte, M. Youssef, S. Sacanna, A. Donev, P. Chaikin, *Nat. Phys.* **2017**, *13*, 375.

[30] B. Delmotte, M. Driscoll, P. Chaikin, A. Donev, *Phys. Rev.* **2017**, *2*, 092301.

[31] T. Beatus, T. Tlusty, R. Bar-Ziv, *Phys. Rev. Lett.* **2009**, 103, 114502 .

[32] B. Delmotte, *Phys. Rev.* **2019**, *4*, 044302.

[33] H. Massana-Cid, E. Navarro-Argemí, D. Levis, I. Pagonabarraga, P. Tierno, *J. Chem. Phys.* **2019**, *150*, 164901.

[34] A. Kaiser, A. Snezhko, I. Aranson, *Sci. Adv.* **2017**, *3*, e1601469.

[35] Y. Wang, S. Canic, G. Kokot, A. Snezhko, I. Aranson, *Phys. Rev.* **2019**, *4*, 013701.

[36] G. Kokot, A. Vilfan, A. Glatz, A. Snezhko, *Soft Matter* **2019**, *15*, 3612–3619.

[37] F. Martinez-Pedrero, A. Ortiz-Ambriz, I. Pagonabarraga, P. Tierno, *Phys. Rev. Lett.* **2015**, *115*, 138301.

[38] a) A. Cebers, H. Kalis, *Eur. Phys. J. E* **2011**, *34*, 1292; b) X. J. A. Janssen, A. J. Schellekens, K. van Ommering, L. van IJzendoorn, M. W. J. Prins, *Bios.* Bioel. **2009**, *24*, 1937.

[39] F. Martinez-Pedrero, P. Tierno, *Phys. Rev. Appl.* **2015**, *3*, 051003.

[40] H. Massana-Cid, F. Meng, D. Matsunaga, R. Golestanian, P. Tierno, *Nat. Commun.* **2019**, *10*, 2444.

[41] a) P. Tierno, R. Muruganathan, T. M. Fischer, *Phys. Rev. Lett.* **2007**, *98*, 028301; b) J. Černák, G. Helgesen, *Phys. Rev. E* **2008**, *78*, 061401; c) J. Yan, S. C. Bae, S. Granick, *Soft Matter* **2015**,*11*, 147–153; d) D. Du, M. Doxastakis, E. Hilou, S. L. Biswal, *Soft Matter* **2017**, *13*, 1548–1553.

[42] G. Kokot, A. Snezhko, *Nat. Commun.* **2018**, *9*, 2344.

[43] G. Kokot, A. Sokolov, A. Snezhko, *Langmuir* **2019**, *36*, 6957–6962.

[44] K. Han, G. Kokot, O. Tovkach, A. Glatz, I. Aranson, A. Snezhko, *Proc. Natl. Acad. Sci. USA* **2020**, *117*, 9706–9711.

[45] K. Han, A. Snezhko, *Lab Chip* **2021**, *21*, 215–222.

[46] G. Kokot, D. Piet, G. M. Whitesides, I. Aranson, A. Snezhko, *Sci. Rep.* **2015**, *5*, 9528.

[47] a) G. Kokot, S. Das, R. G. Winkler, G. Gompper, I. Aranson, A. Snezhko, *Proc. Natl. Acad. Sci. USA* **2017**, *114*, 12870–12875; b) A. Snezhko, I. Aranson, *Soft Matter* **2015**, *11*, 6055–6061.

[48] K. Han, G. Kokot, S. Das, R. G. Winkler, G. Gompper, A. Snezhko, *Sci. Adv.* **2020**, *6*, eaaz8535.

[49] B. Grzybowski, H. Stone, G. M. Whitesides, *Nature* **2000**, *405*, 1033–1036.

[50] D. Matsunaga, J. K. Hamilton, F. Meng, N. Bukin, E. L. Martin, F. Y. Ogrin, J. M. Yeomans, R. Golestanian, *Nat. Commun.* **2019**, *10*, 4696.

[51] A. Liberzon, R. Gurka, G. Hetsroni, *Exp. Fluids* **2004**, *36*, 355–362.

[52] A. Terray, J. Oakey, D. W. M. Marr, *Science* **2002**, *296*, 1841.

[53] P. Tierno, S. V. Reddy, J. Yuan, T. H. Johansen, T. M. Fischer, *J. Phys. Chem. B* **2007**, *111*, 13479–13482.

[54] A. Chamolly, E. Lauga, S. Tottori, *Soft Matter* **2020**, *16*, 2611.

[55] H. Massana-Cid, F. Martinez-Pedrero, E. Navarro-Argemí, I. Pagonabarraga, P. Tierno, *New J. Phys.* **2017**, *19*, 103031.

[56] N. Casic, N. Quintero, R. A. Nodarse, F. G. Mertens, L. Jibuti, W. Zimmermann, T. M. Fischer, *Phys. Rev. Lett.* **2013**, *110*, 168302.

[57] T. R. Kline, W. F. Paxton, T. E. Mallouk, A. Sen, *Angew. Chem. Int. Ed.* **2005**, *44*, 744.

[58] V. Garcia-Gradilla, J. Orozco, S. Sattayasamitsathit, F. Soto, F. Kuralay, A. Pourazary, A. Katzenberg, W. Gao, Y. Shen, J. Wang, *ACS Nano* **2013**, *7*, 9232–9240.

[59] M. Han, J. Yan, S. Granick, E. Luijten, *Proc. Natl. Acad. Sci. USA* **2017** *114*, 7513–7518.

[60] F. Martinez-Pedrero, H. Massana-Cid, P. Tierno, *Small* **2017**, *13*, 1603449.

[61] P. Tierno, R. Albalat, F. Sagués, *Small* **2010**, *6*, 1749–1752.

[62] J. Palacci, S. Sacanna, A. P. Steinberg, D. J. Pine, P. M. Chaikin, *Science* **2013**, *339*, 936.

[63] J. C. Crocker, D. G. Grier, *J. Colloid Interface Sci.* **1996**, *179*, 298–310.

[64] T. M. Squires, S. R. Quake, *Rev. Mod. Phys.* **2005**, *77*, 977.

[65] G. M. Whitesides, *Nature* **2006**, *442*, 368–373.

[66] J. P. Steimel, J. L. Aragones, A. Alexander-Katz, *Phys. Rev. Lett.* **2014**, *113*, 178101.

[67] a) F. Martinez-Pedrero, A. Cebers, P. Tierno, *Phys. Rev. Appl.* **2016**, *6*, 034002; b) T. Yang, T. O. Tasci, K. B. Neeves, N. Wu, D. W. M. Marr, *Langmuir* **2017**, *33*, 5932–5937.

[68] a) G. Grosjean, G. Lagubeau, A. Darras, M. Hubert, G. Lumay, N. Vandewalle, *Sci. Rep.* **2015**, *5*, 16035; b) D. Du, E. Hilou, S. L. Biswal, *Soft Matter* **2018**, *14*, 3463; c) M. Vilfan, N. Osterman, A. Vilfan, *Soft Matter* **2018**, *14*, 3415.

[69] Y. Dou, P. M. Tzelios, D. Livitz, K. J. M. Bishop, *Soft Matter* **2021**, *17*, 1538–1547.